Nguyen, D. H., Lowenberg , M. H., Neild, S. A., & Richardson, T. S. (2021). Transient Dynamics Assessment of a Gain-Scheduled Aircraft Controller Using Nonlinear Frequency Approach. *Journal of Guidance, Control, and Dynamics*, *44*(9), 1692-1699. https://doi.org/10.2514/1.G005866

Transient Dynamics Assessment of a Gain-Scheduled Aircraft Controller Using Nonlinear Frequency Approach

Duc H. Nguyen[1], Mark H. Lowenberg[2], Simon A. Neild[3], and Thomas S. Richardson[4]

Department of Aerospace Engineering, University of Bristol, Bristol, BS8 1TR

Nomenclature

A = forcing amplitude (deg)

C_Z, C_M = force and moment coefficients

f = forcing frequency (Hz)

q = pitch rate (deg/s)

t = time (s)

u = general input vector

x = general state vector

α = angle of attack (deg)

η = elevator deflection (deg)

Λ = proportional gain

ω = forcing frequency (rad/s)

Subscripts

d = demanded

0 = value at trimmed (steady) flight

[1] PhD student, AIAA Student Member.
[2] Professor of Flight Dynamics, AIAA Senior Member.
[3] Professor of Nonlinear Structural Dynamics.
[4] Professor of Aerial Robotics, AIAA Senior Member.

I. Introduction

Although many existing controller design techniques and flying qualities criteria are linear-based [1, 2], the influence of the nonlinear elements, especially at high angles-of attack, can degrade the performance to the point that it no longer resembles the predictions made by linear analysis [3, 4]. Even when the local nonlinear performance is satisfactory, there is no guarantee that the dynamics remains consistent as the aircraft transitions across different operating points [4]. Therefore, a full-envelope aircraft controller requires extensive testing to verify its performance across the entire operating envelope. This is a time-consuming process [5], and there is currently no systematic method to quantify the performance degradation due to the nonlinear terms.

In an effort to bridge the gap between the linear and nonlinear domains, there has been increasing interest in utilizing bifurcation theory with numerical continuation in the flight dynamics and control context [3-7]. Bifurcation analysis generates a map of the steady-state solutions as a parameter, such as elevator deflection or a controller gain, is varied. Highly nonlinear steady-state behaviors like spin and autorotation can be identified and characterized as either stable or unstable solutions. This approach has its limits, most notably the inability to capture the non-stationary elements such as damping, frequency-domain modal coupling, and the influence of gain scheduling associated with equilibrium solutions. In practical terms, this means bifurcation analysis is very useful in identifying regions where the dynamics is unstable and should be avoided, but not in assessing an aircraft performance during transient motion between different stable solutions. To develop this aspect of the analysis, there have been some investigations into studying the periodically-forced response by coupling the aircraft with a harmonic oscillator [8-10]. This approach was recently expanded into the 'nonlinear frequency response' method in a flight dynamics context [11], which is capable of detecting many non-stationary phenomena that seriously degrade flying qualities and contribute to pilot-induced oscillation [12].

This note aims to further exploit the advantages of the method in [11] to identify regions with degraded flying qualities that have gone undetected by linear analysis. This is based on the premise that if the frequency responses at different operating points look similar, then their time-domain responses must also be similar, and vice versa. In addition, as periodically forced systems are non-stationary by definition, the proposed approach can reveal the influence of the nonlinear and non-stationary terms, such as aerodynamic damping and scheduled gains, which all have an effect on the aircraft during its transient motion.

In this note, nonlinear frequency response analysis is conducted using the Dynamical Systems Toolbox [13], which is an implementation of the numerical continuation software AUTO [14] in the MATLAB/Simulink environment. Detailed explanation of the method can be found in [11].

II. Plant and Controller Architecture

A. Aircraft model

The method proposed in this note is demonstrated on the Hypothetical High Angle of Incidence Research Model (HHIRM), which was originally created for nonlinear flight dynamics studies in the Defence Research Agency in the UK (now QinetiQ) [15]. The model is made up of six aerodynamic force and moment coefficients represented as nonlinear spline functions of the angle of attack, sideslip angle, angular rates, and control surface deflections. Its dynamics are representative of a typical fighter aircraft. The use of spline functions rather than tabular data ensures that the system is smooth (differentiable), making the model highly suitable to be used as a testbed for bifurcation-based methods. Further description of the force and moment coefficients can be found in [15, 16]. In this note, the longitudinal 2nd-order version is used (the same approach adopted in [4]), which contains two states α (angle of attack in degrees) and q (pitch rate in degrees/s) to capture the short-period mode. Using the reduced-order model restricts the case study to longitudinal dynamics, where only the fast mode is important, and allows for easier interpretation of the results. However, the approach developed in this note is not limited to such low-order systems.

The equations of motions for the open-loop aircraft are:

$$\dot{\alpha} = \frac{\rho V S}{2m}\left[C_Z(\alpha) + \eta C_{Z_\eta}(\alpha) + \frac{qc}{2V} C_{Z_q}(\alpha)\right]\cos(\alpha) + q \tag{1}$$

$$\dot{q} = \frac{\rho V^2 S c}{2I_y}\left[C_M(\alpha) + \eta C_{M_\eta}(\alpha, \eta) + \frac{qc}{2V} C_{M_q}(\alpha)\right] \tag{2}$$

Table 1 lists the values of the physical parameters in equations (1-2), and Fig. 1 shows the nonlinear aerodynamic coefficients.

Table 1 Aircraft parameters

ρ	air density at 5,000 m	0.7358 kg/m^3
V	total velocity	150 m/s
S	wing area	37.16 m^2
c	mean aerodynamic chord	3.511 m
m	mass	15,000 kg
I_y	pitch moment of inertia	163,280 kg m^2

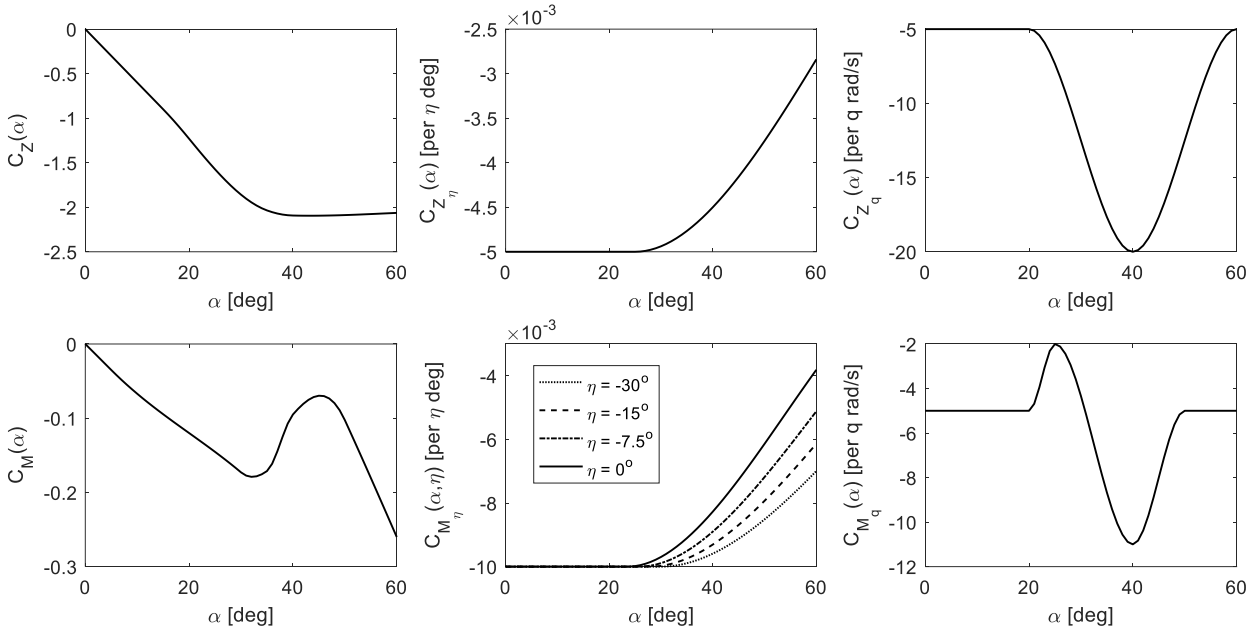

Fig. 1 Aerodynamic coefficients and derivatives.

The open-loop dynamics of the HHIRM has been studied using conventional bifurcation analysis [4] and is briefly reproduced here for completeness. Regarding the method, bifurcation analysis provides the steady-state solutions to the equation $\dot{\boldsymbol{x}} = f(\boldsymbol{x}, \boldsymbol{u})$, where $\boldsymbol{x}$ is the state vector and $\boldsymbol{u}$ is the input vector. To determine the relationship between $\boldsymbol{x}$ and $\boldsymbol{u}$ when $\dot{\boldsymbol{x}} = \boldsymbol{0}$, we solve the equation $\dot{\boldsymbol{x}} = \boldsymbol{0}$ with $\boldsymbol{u}$ as the continuation parameter using the numerical continuation methods [17], then present the result in a bifurcation diagram. For the HHIRM, Fig. 2 shows the open-loop bifurcation diagrams of the two states α and q with the elevator deflection η on the x-axis as the continuation parameter. These diagrams are the equilibria sets for the two states α and q as functions of η. The line type indicates local stability: solid line type denotes stable equilibria and dashed means unstable. It can be seen that due to the fold

bifurcations, the flight dynamics can be divided into three separate regions as illustrated in Fig. 2a. From a practical perspective, this means that:

- For $-20^o \leq \eta \leq -10^o$, the aircraft has two stable equilibrium states: one at a lower and one at a higher (deep stall) angle of attack. Whichever solution the aircraft converges to will depend on the initial conditions in a time history simulation or on the magnitude of disturbances.

- It is not possible to manually trim the aircraft at angles-of-attack between 34^o and 46^o because the solutions in that range are unstable. Note that this corresponds to the static instability reflected in the region of positive pitching moment slope of $C_{M_\alpha}(\alpha)$ in Fig. 1.

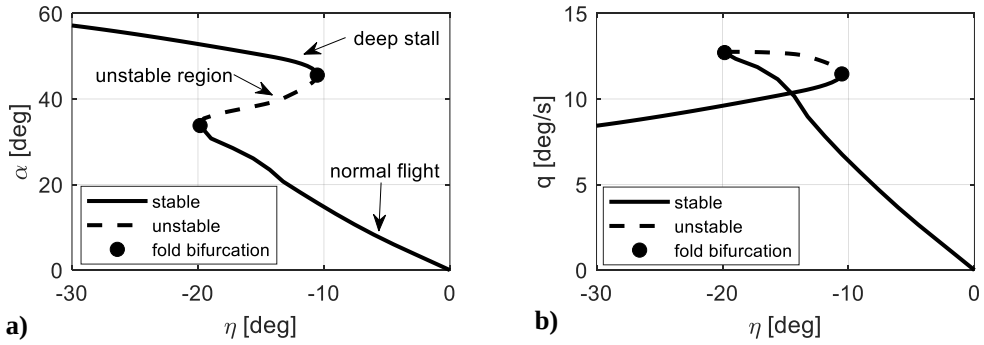

Fig. 2 Open-loop bifurcation diagram – elevator continuation.

B. Description of the input gain-scheduled controller

In the analysis to follow, the closed-loop HHIRM uses the longitudinal version of the gain-scheduled controller described in [18]. This is essentially a state-feedback controller with an integral term in the forward path to create a maneuver-demand system while also accounting for the dynamics of a first-order actuator. The block diagram and gain scheduling are shown in Fig. 3. All three controller gains are scheduled against the pilot's input α_d (demanded angle-of-attack), hence the term input gain scheduling. The objective of the controller is to place the short-period and integrator poles at fixed locations throughout the entire operating envelope to achieve consistent level 1 handling qualities. Figure 4a shows the pole positions in the complex plane at each operating point from 0^o to 60^o angle-of-attack at 1^o interval. The linear analyses were done by linearising the open-loop aircraft at 61 different values of η that give α = [0^o, 1^o, 2^o, …, 60^o], then adding the actuator and controller with the gains as shown in Fig. 3b. It can be seen that the design objective of fixing the pole positions is achieved. Further verifications of linear-based analysis are

shown in the linear step and frequency responses (Fig. 4b and 4c). Since the responses are almost identical in all cases, it can be said that the aircraft exhibits consistent handling qualities across the entire operating envelope (in terms of pole positions). As far as linear design goes, this is a best case scenario, especially when gain scheduling in most real aircraft is done at much larger intervals.

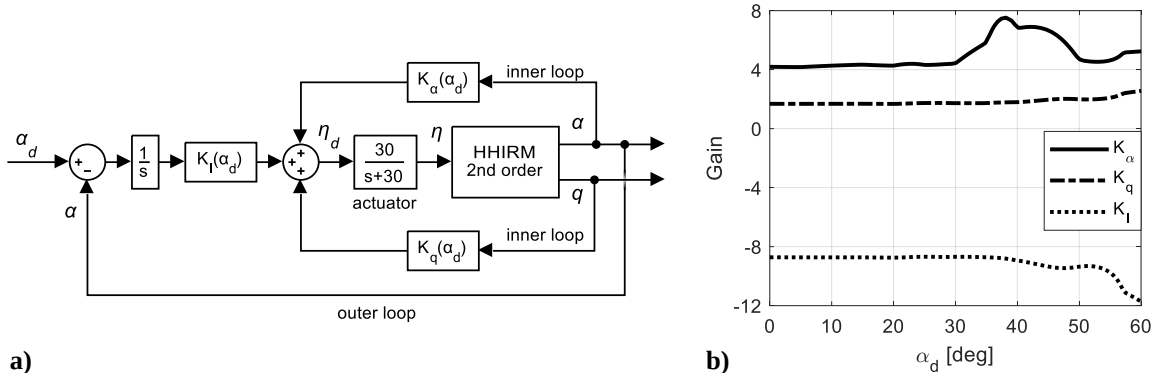

Fig. 3 Block diagram (a) and gain scheduling (b) – state feedback controller with integral action.

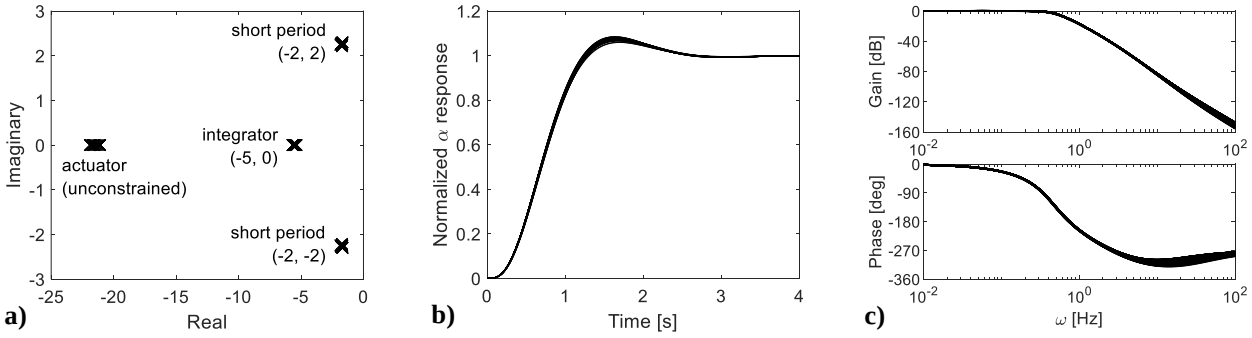

Fig. 4 Linear analysis: closed-loop poles (a), unit step responses (b), and closed-loop frequency responses (c) at every operating point.

Finally, Fig. 5 shows the equilibrium solutions of the closed-loop aircraft as the pilot input α_d varies. This figure was generated using numerical continuation with α_d as the continuation parameter. The slope of 1 in the α bifurcation diagram shows that in addition to achieving zero steady-state error, the controller has also ensured that there is no other attractor near the intended operating range. Thus far, the system looks promising as not only does the aircraft exhibit the desired characteristic of a maneuver-demand system, but also that conventional bifurcation analysis indicates no potential issue arising from the presence of nonlinearities.

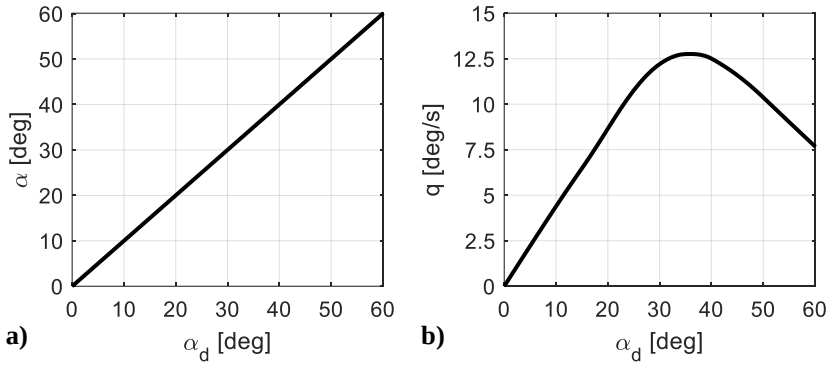

Fig. 5 Closed-loop bifurcation diagrams of angle-of-attack (a) and pitch rate (b) against the pilot input.

III. Nonlinear Analysis: Issues with Input Gain Scheduling

A. Time and frequency responses

Fig. 6 shows the step responses of the nonlinear HHIRM to a range of step inputs (i.e., stepping from α_0 to α_d). We define the normalized α response as $(\alpha - \alpha_0)/(\alpha_d - \alpha_0)$. This was done to scale the initial and final values to 0 and 1, making it easier to compare the linear and nonlinear responses. Cases A and B in Fig. 6 are almost identical, despite the large input of 15° in case B, and their dynamics resemble the linear responses in Fig. 4b. However, as the initial value of α increases to 21° (case C), the step response starts to differ from those seen previously as well as the linearized responses. In case D, a small 1° step from 30° angle-of-attack results in an initial undershoot before the elevator movement reverts back to the correct direction. This behavior is not detected using linear analysis and at first glance may resemble non-minimum phase behavior. However, the cause is attributed to the aerodynamic nonlinearities of the model. Figure 1 shows that the slopes of $C_Z(\alpha)$ and $C_M(\alpha)$ reverse direction at around 30 degrees angle-of-attack, which is combined with a gradual loss of elevator effectiveness above α = 30° as seen in the plots for $C_{Z_\eta}(\alpha)$ and $C_{M_\eta}(\alpha, \eta)$. Additionally, larger step inputs that cross this region will also be affected by the issues related to

scheduling of the gains against the reference signal. A step input causes an instantaneous change in the gain values, and Fig. 3b shows that beyond 30° angle-of-attack, the gains vary considerably (especially for K_α). On the other hand, the aircraft states do not change as rapidly so at the beginning of the maneuver, there is a mismatch between the values of the current states and the optimal gain values.

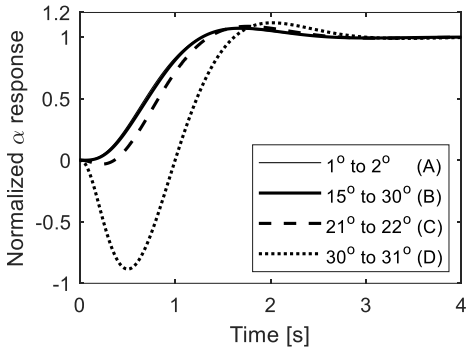

Fig. 6 Response of nonlinear model to step inputs.

It has been shown that input gain scheduling may result in nonlinear dynamics that can only be observed during the transient phase. As existing methods like linear time/frequency-domain analysis and conventional bifurcation methods cannot capture these dynamics, we propose using an extension of bifurcation analysis to investigate these behaviors. Specifically, we will examine the aircraft's nonlinear frequency responses to a periodic forcing of the pilot input. This is done by augmenting the current fourth-order system ($[\alpha, q, \eta, integrator]$) with a harmonic oscillator described by the following equations:

$$\dot{x}_5 = x_5 + \omega x_6 - x_5(x_5^2 + x_6^2) \tag{3}$$

$$\dot{x}_6 = x_6 - \omega x_5 - x_6(x_5^2 + x_6^2) \tag{4}$$

where ω is the forcing frequency in rad/s. It can be shown that $x_5 = \sin(\omega t)$ and $x_6 = \cos(\omega t)$. The pilot input now takes the form:

$$\alpha_d = \alpha_0 + A\sin(\omega t) = \alpha_0 + Ax_5 \tag{5}$$

where A (deg) is the forcing amplitude and α_0 (deg) is the pilot input when there is no harmonic forcing.

Figure 7 shows the frequency responses at α_0 = 30° and A = 1°. These values are chosen to match the step response from 30° to 31° seen in Fig. 6. Similar to the step responses, there is a notable discrepancy between the linear and nonlinear frequency responses. As the forcing frequency $f = \omega/2\pi$ (in Hz) increases, the nonlinear frequency response has higher gain but lower phase compared to its linearized counterpart. This suggests that neither an additional pole

nor a zero in the linear transfer function could correct their differences. We can therefore conclude that the dynamics in this region cannot be captured by a linear transfer function, which matches the highly nonlinear behavior seen in the step responses from 30° to 31°.

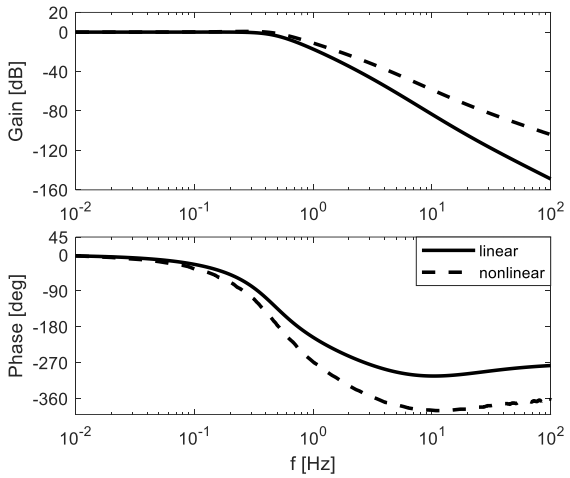

Fig. 7 Closed-loop frequency response at α_0 = 30° and A = 1°.

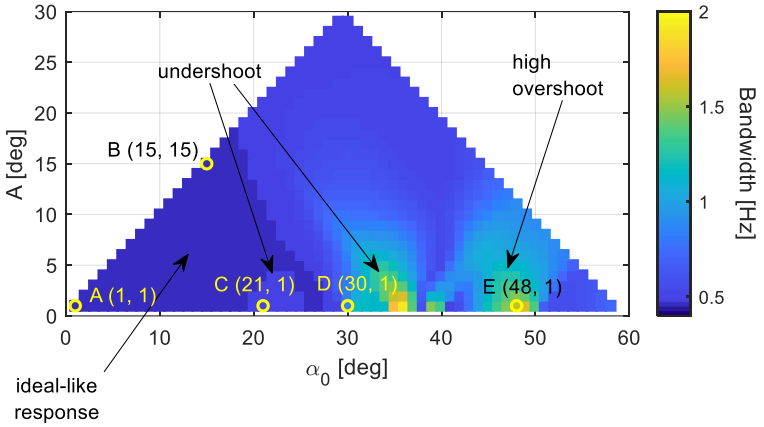

Fig. 8 Closed-loop bandwidth variation – feedback with integral action controller.

The linear analysis in Figs. 4b and 4c has shown that if the frequency responses at different operating points are similar, then their step responses are also similar. Based on this assumption, we can make predictions on the aircraft dynamics when it transitions between different operating points in response to a large step input. This is done by generating the nonlinear frequency response for a range of α_0 and A and comparing their bandwidths – defined here as the frequency at which the gain drops to –3 dB. The result is shown as a scatterplot in Fig. 8, which has the triangular shape because the controller is only designed for α_d between 0° and 60° (as a reminder, $\alpha_d = \alpha_0 + A\sin(2\pi ft)$ for

the forced response). The lower-left section of Fig. 8 has similar coloration and therefore suggests similar dynamics. This is expected, as points A (1°, 1°) and B (15°, 15°) are related to the step responses from 1° to 2° and 15° to 30°, which are indeed similar as shown in Fig. 6. On the other hand, points C and D (also labelled accordingly in both Fig. 8 and Fig. 6) exhibit different dynamics, and this is reflected by their differences in the frequency responses comparing to points A and B. Although the aircraft can have different responses to a range of inputs, the triangular plot in Fig. 8 gives us an indication of where the dynamics may be comparable.

In addition to the undershoot behavior as discussed, there is an apparent separate nonlinear region around point E in Fig. 8. We investigate this by generating the frequency and step responses at point E (48°, 1°). Figure 9a shows that the nonlinear frequency response has a notably higher resonance gain than the linear prediction, suggesting that the nonlinear step response will have a much higher overshoot, a fact confirmed in Fig. 9b. The higher resonance leads to an increase in bandwidth, which is reflected by the area around point E in Fig. 8. Based on the shape of the nonlinear frequency response, it is inferred that the linearized response needs an additional zero in its transfer function in order to capture the dynamics correctly.

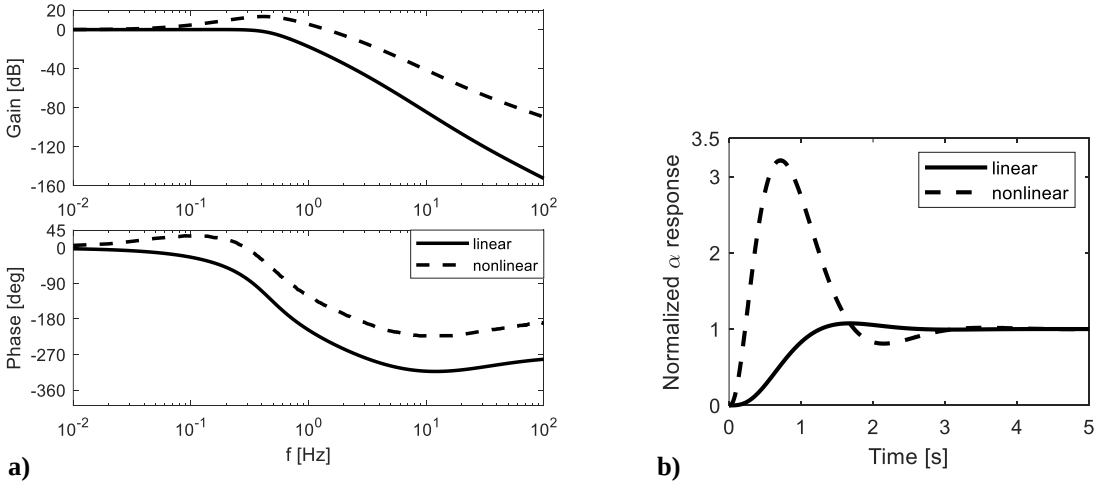

Fig. 9 (a) frequency response at α_0 = 48° and A = 1° and (b) step response from 48° to 49°.

A physical explanation for the nonlinear dynamics observed can be inferred by linking the triangular envelope with the open-loop α bifurcation diagram in Fig. 2a. We note that the nonlinear dynamics surrounding points D and E in Fig. 8 involves the aircraft traversing near or past the fold bifurcations at 34° and 46°. Each time a fold bifurcation is crossed, the relationship between α and η is reversed. The direct consequence is that in order to follow the sinusoidal input of α_d, the elevator movement must change direction during the maneuver. This element is not accounted for in

linear pole-placement design, which contributed to the undesirable responses observed. Figure 10 shows one example of a simple sinusoidal α_d input that results in very complex variations of both α and η.

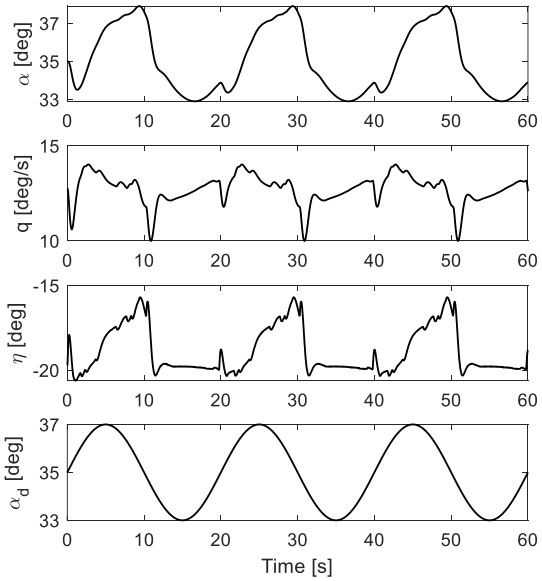

Fig. 10 Nonlinear forced response (f = 0.05 Hz).

Using nonlinear frequency response analysis, we have presented a method to verify whether consistent handling qualities are achieved across different operating regions. The result has highlighted the issues associated with input gain scheduling, especially when strong nonlinearities are present. It is important to point out that the purpose of the triangular envelope is not to compare the closed-loop bandwidth in responses to different values of α_0 and A, but to indicate that bandwidth might be used as a metric to quantify the differences in the frequency response at different operating points. For a more complex system with multiple peaks, the engineer might apply a different metric, such as resonance peak or estimated damping of each mode, depending on the application considered.

B. Validating the gain margin predictions from linear analysis

To further highlight how conventional linear-based design methods can be deleteriously affected by the nonlinear phenomena discussed above, we will verify the gain margin predictions of the open-loop frequency response. In this case, the open-loop system is defined by removing the outer loop in Fig. 3a while keeping the inner stability-augmentation loops with $K_\alpha(\alpha_d)$ and $K_q(\alpha_d)$ unchanged. The gain margins of the open-loop transfer functions at each operating point are plotted as the solid thin line in Fig. 11a. To do the same calculation on the nonlinear system, we use the scheme in Fig. 12a, which is the closed-loop system seen in Fig. 3a augmented with a proportional gain Λ

before the integrator, then do conventional bifurcation analysis (without the harmonic oscillator) with Λ as the continuation parameter. An example of Λ continuation is shown in Fig. 13 at 30° angle-of-attack. As Λ increases, the system becomes unstable at Λ = 4.48 via a Hopf bifurcation. Beyond this value, any perturbation from the trim point will send the aircraft into an unstable limit cycle. In this example, Λ = 4.48 is the 'nonlinear gain margin'. Λ is calculated at each operating point of the nonlinear system (which can be done manually or by using two-parameter continuation of the Hopf bifurcation – the latter is much more computationally efficient) and plotted in Fig. 11a as a thick dashed line. In this instance, the linear predictions are correct.

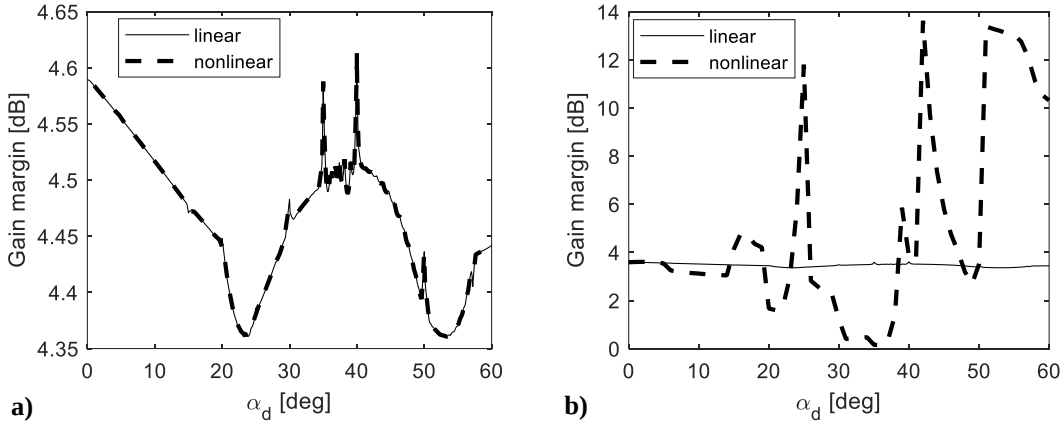

Fig. 11 Gain margin variation of (a) the controller with integral path and (b) the simple pilot-vehicle system.

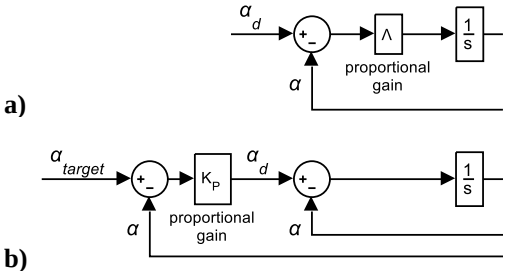

Fig. 12 Block diagrams for gain margin calculation: gain-scheduled controller (a) and simple pilot-vehicle system (b).

Although the linear gain margin obtained from the open-loop transfer function appears accurate, we have seen in Section III-A that there are cases in which the linear and nonlinear closed-loop frequency responses differ significantly. This suggests that the gain margin predictions from these closed-loop frequency responses can be incorrect. To assess the accuracy of these predictions, we remove Λ and add an additional outer loop to the controller along with a proportional gain K_P, resulting in the system shown in Fig. 12b. From a physical perspective, the

proportional gain K_P can be considered a simple pilot model and the input signal will be the target angle-of-attack for the pilot to track. Again, we trim the aircraft and conduct unforced bifurcation analysis with K_P as the continuation parameter, find the locus of the Hopf bifurcation as α_0 varies, then compare the result with the linear analysis. Figure 11b shows that the linear and nonlinear gain margins now differ significantly beyond α_0 = 5º, which is a very low angle-of-attack, and suggests that each time a loop is closed, the effect of nonlinearities increases considerably. This can have serious consequences when more complex components are added to the analysis, such as a more realistic nonlinear pilot model or a rate and travel-limited actuator.

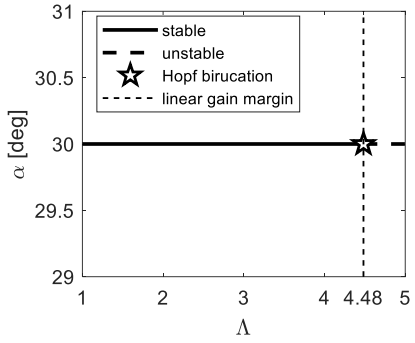

Fig. 13 Bifurcation diagram of α with Λ continuation.

It has been shown that aerodynamic nonlinearities can negatively affect the aircraft's responses in both the time and the frequency domains, in a way that linear-based design (including input gain scheduling) cannot anticipate. The next section will further utilize the nonlinear frequency response method to analyze a different controller scheme, which promises to address some of the challenges associated with input gain scheduling.

IV. Analysis of the Dynamic Gain Scheduled Controller

For the final study, we further validate the proposed nonlinear frequency method by examining the performance of the dynamic gain scheduled controller for the HHIRM in [19]. Dynamic gain scheduling in this case involves determining the gains using eigenstructure assignment (effectively pole placement in this model) and scheduling them against the fast-varying states rather than the slow-varying ones or the input while accounting for the effect of this on the local stability (Jacobian matrix). This novel method of nonlinear control design shows superior performance to conventional input gain scheduling [19-22], and is further examined here to ensure that our proposed method does not generate false-positive results (i.e. indicating a problem when there is none). The controller schematic is similar to

Fig. 3a, except that the inner-loop gains are now scheduled against their respective states (i.e. $K_\alpha(\alpha_d)$ and $K_q(\alpha_d)$ become $K_\alpha(\alpha)$ and $K_q(q)$). Figure 14 plots these gains, which were taken directly from the data in [19]. It has been noted in [19] that although $K_\alpha(\alpha)$ is available for the entire operating envelope from 0° to 60° angle-of-attack, $K_q(q)$ was only calculated up to q = 12.75° (the value at α_d = 36°) due to a fold bifurcation that leads to a non 1:1 mapping between $K_q(q)$ and q. In Fig. 14b, the relationship between q and α_d can be seen in the secondary x-axis, which maps q on the main x-axis to the pilot input required to achieve that value of q at steady state. Therefore, full dynamic gain scheduling is only available for α_d below 36°. Above this value, K_α is still dynamically scheduled whereas K_q is fixed at its maximum calculated value of 1.702.

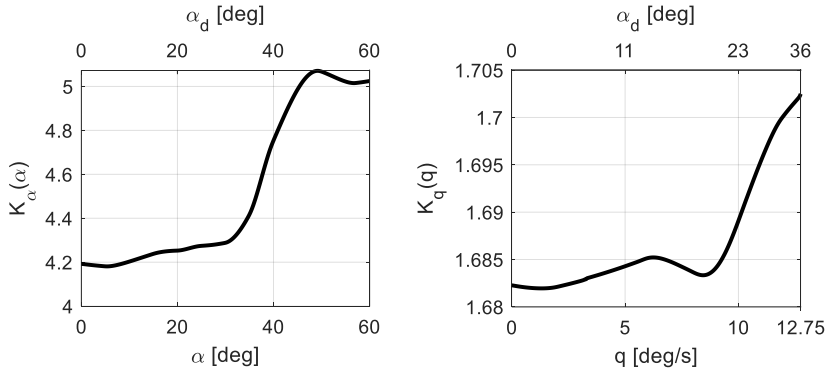

Fig. 14 Dynamic gain schedules.

As before, we use nonlinear frequency response analysis again to compare the closed-loop bandwidths at different operating points. The result is shown in Fig. 15a, which uses the same color mapping as Fig. 8. A boundary is defined to separate regions with full and partial dynamic gain scheduling. There is a region of missing data points in Fig. 15a at very high angles-of-attack. In these instances, the continuation algorithm failed to solve, potentially because larger K_q is required to prevent the aircraft from diverging. Despite the lack of scheduling data, it can be seen that the performance is more consistent across the entire envelope than in Fig. 8. Specifically, points F (15°, 15°) and G (30°, 1°) now have similar bandwidth, and the undershooting previously seen at point D in Fig. 6 and Fig. 8 is no longer an issue based on the time simulation of point G in Fig. 15b. The triangular envelope also indicates that points H (a very demanding input) and I have slightly different dynamics comparing to points F and G. Their step responses in Fig. 15b show that although this is the case, the effect is minimal, and that the overall performance is much more consistent across the entire envelope when compared to input gain scheduling. This confirms the observation made in [19] that dynamic gain scheduling gives improved transient performance and can address the problems encountered in input

gain scheduling with fast-varying state variables, especially when the aircraft maneuvers rapidly across different operating points.

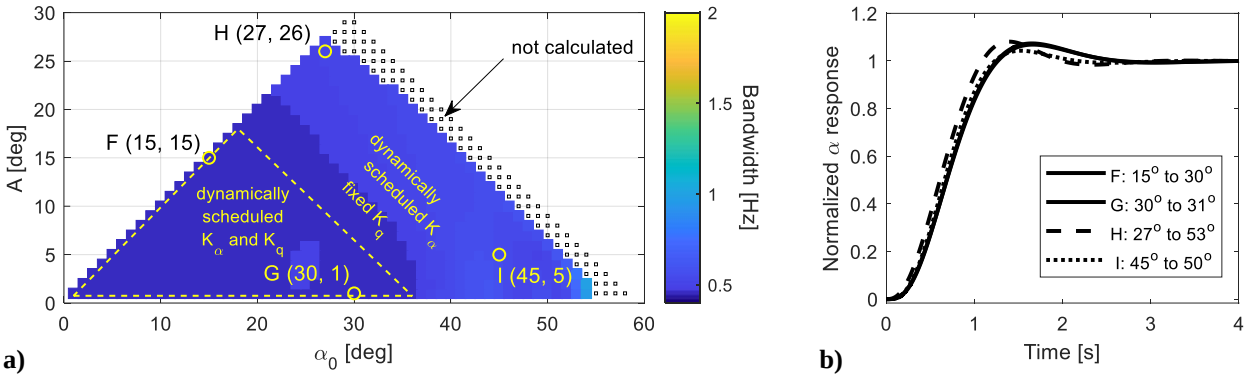

Fig. 15 Dynamic gain scheduled controller: (a) closed-loop bandwidth variation and (b) step responses.

V. Conclusion

This note has presented a method to systematically assess the variation in transient dynamics across different operating points in an aircraft flight envelope. Using nonlinear frequency response analysis, it is possible to identify regions with degraded flying qualities that have gone undetected by linear-based methods. In the examples presented, the combination of aerodynamic nonlinearities and input gain scheduling leads to undesirable responses like undershoot and overshoot. We have also shown that the discrepancies between the linear and nonlinear frequency responses can lead to erroneous gain margin predictions. These errors are magnified each time a feedback loop is closed, which can have serious consequences in a complex system with many loops and nonlinear components. Finally, we used the method to verify the superior performance of a dynamic gain-scheduled controller relative to a standard implementation of scheduling gains with an input or slow variable, since dynamic gain scheduling provides consistent transient response across the entire envelope. Nonlinear frequency response analysis therefore provides a means of gaining insight into potential degradations in performance and handling qualities when a controller designed using linear techniques is applied to a highly nonlinear system.

Acknowledgements

The first author is partially funded by the University of Bristol's Alumni Grant. The support of QinetiQ in providing the HHIRM flight model is also gratefully acknowledged.

References

1. Annonymous. "Military Specification - Flying Qualities of Piloted Airplanes." US Department of Defense, TR-MIL-F-8785C, 1980.

2. Gibson, J. C. "The development of alternative criteria for FBW handling qualities", *AGARD Conference Proceedings No. 508*, AGARD Paper 9, 1991.

3. Gill, S. J., Lowenberg, M. H., Neild, S. A., Crespo, L. G., Krauskopf, B., and Puyou, G. "Nonlinear Dynamics of Aircraft Controller Characteristics Outside the Standard Flight Envelope", *Journal of Guidance, Control, and Dynamics*, Vol. 38, No. 12, 2015, pp. 2301-2308.
doi: 10.2514/1.G000966

4. Richardson, T., Lowenberg, M., Di Bernardo, M., and Charles, G. "Design of a Gain-Scheduled Flight Control System Using Bifurcation Analysis", *Journal of Guidance, Control, and Dynamics*, Vol. 29, No. 2, 2006, pp. 444-453.
doi: 10.2514/1.13902

5. Macmillen, F. B. J., and Thompson, J. M. T. "Bifurcation analysis in the flight dynamics design process? A view from the aircraft industry", *Philosophical Transactions of the Royal Society of London. Series A: Mathematical, Physical and Engineering Sciences*, Vol. 356, No. 1745, 1998, pp. 2321-2333.
doi: 10.1098/rsta.1998.0276

6. Carroll, J. V., and Mehra, R. K. "Bifurcation Analysis of Nonlinear Aircraft Dynamics", *Journal of Guidance, Control, and Dynamics*, Vol. 5, No. 5, 1982, pp. 529-536.
doi: 10.2514/3.56198

7. Lowenberg, M. H. "Bifurcation analysis of multiple–attractor flight dynamics", *Philosophical Transactions of the Royal Society of London. Series A: Mathematical, Physical and Engineering Sciences*, Vol. 356, No. 1745, 1998, pp. 2297-2319.
doi: 10.1098/rsta.1998.0275

8. Mehra, R. K., and Prasanth, R. K. "Bifurcation and limit cycle analysis of nonlinear pilot induced oscillations", *23rd Atmospheric Flight Mechanics Conference*, AIAA Paper 98-4249, 1998.
doi: 10.2514/6.1998-4249

9. Gránásy, P., Thomasson, P. G., Sørensen, C. B., and Mosekilde, E. "Non-linear flight dynamics at high angles-of-attack", *The Aeronautical Journal*, Vol. 102, No. 1016, 1998, pp. 337-344.
doi: 10.1017/S0001924000027585

10. Lowenberg, M., and Menon, P. "An Analysable Nonlinear Criterion for Clearance of Flight Control Laws", *AIAA Guidance, Navigation and Control Conference and Exhibit*, AIAA Paper 2007-6507, 2007.
doi: 10.2514/6.2007-6507

11. Nguyen, D. H., Lowenberg, M. H., and Neild, S. A. "Frequency-Domain Bifurcation Analysis of a Nonlinear Flight Dynamics Model", *Journal of Guidance, Control, and Dynamics,* Vol. 44, No. 1, 2020, pp. 138-150. doi: 10.2514/1.G005197

12. Nguyen, D. H., Lowenberg, M. H., and Neild, S. A. "Effect of Actuator Saturation on Pilot-Induced Oscillation: a Nonlinear Bifurcation Analysis", *Journal of Guidance, Control, and Dynamics*, 2021. doi: 10.2514/1.G005840

13. Coetzee, E., Krauskopf, B., and Lowenberg, M. H. "The Dynamical Systems Toolbox: Integrating AUTO into Matlab", *16th US National Congress of Theoretical and Applied Mechanics*, Pennsylvania State University Paper USNCTAM2010-827, 2010.

14. Doedel, E. J. "*AUTO-07P, Continuation and Bifurcation Software for Ordinary Differential Equations, Ver. 07P*", http://www.macs.hw.ac.uk/~gabriel/auto07/auto.html [retrieved 24 March 2021].

15. Goman, M., Khramtsovsky, A., and Usoltev, S. "High Incidence Aerodynamics Model for Hypothetical Aircraft," *Technical Rept. 15/5DRA*. Defense Research Agency, Bedford, Bedfordshire, England, UK, 1995.

16. Goman, M. G., and Khramtsovsky, A. V. "Application of continuation and bifurcation methods to the design of control systems", *Philosophical Transactions of the Royal Society of London. Series A: Mathematical, Physical and Engineering Sciences,* Vol. 356, No. 1745, 1998, pp. 2277-2295. doi: 10.1098/rsta.1998.0274

17. Krauskopf, B., Osinga, H. M., and Galán-Vioque, J., *Numerical continuation methods for dynamical systems: path following and boundary value problems*, Understanding Complex Systems, chapter 1, Springer, Dordrecht, 2007. doi: 10.1007/978-1-4020-6356-5

18. Richardson, T. S., and Lowenberg, M. H. "A continuation design framework for nonlinear flight control problems", *The Aeronautical Journal,* Vol. 110, No. 1104, 2005, pp. 85-96. doi: 10.1017/s0001924000001032

19. Richardson, T., Davison, P., Lowenberg, M., and Bernardo, M. d. "Control of Nonlinear Aircraft Models Using Dynamic State-Feedback Gain Scheduling", *AIAA Guidance, Navigation, and Control Conference and Exhibit*, AIAA Paper 2003-5503, 2003. doi: 10.2514/6.2003-5503

20. Jones, C. D. C., Lowenberg, M. H., and Richardson, T. S. "Tailored Dynamic Gain-Scheduled Control", *Journal of Guidance, Control, and Dynamics,* Vol. 29, No. 6, 2006, pp. 1271-1281. doi: 10.2514/1.17295

21. Yang, W., Hammoudi, M. N., Herrmann, G., Lowenberg, M., and Chen, X. "Two-state dynamic gain scheduling control applied to an F16 aircraft model", *International Journal of Non-Linear Mechanics*, Vol. 47, No. 10, 2012, pp. 1116-1123. doi: 10.1016/j.ijnonlinmec.2011.09.007

22. Yang, W., Hammoudi, N., Herrmann, G., Lowenberg, M., and Chen, X. "Dynamic gain-scheduled control and extended linearisation: extensions, explicit formulae and stability", *International Journal of Control,* Vol. 88, No. 1, 2015, pp. 163-179. doi: 10.1080/00207179.2014.942881